Article

Not peer-reviewed version

The Ultimate Flexural Strength of Fiber-Reinforced Ceramic Matrix Composite: A Multiscale Approach

Jacques Lamon *

Posted Date: 28 April 2025

doi: 10.20944/preprints202504.2272.v1

Keywords: ceramic matrix composites; fiber; strength; tows; fracture; normal distribution; Weibull

Article

The Ultimate Flexural Strength of Fiber-Reinforced Ceramic Matrix Composite: A Multiscale Approach

Jacques Lamon

LMPS-ENS, Université Paris-Saclay, 4, Avenue des Sciences, CS 30008, 91192 Gif-sur-Yvette, France; jacques.lamon@ens-paris-saclay.fr

Abstract: The paper tackles the important issue of the flexural strength of continuous fibre reinforced ceramic composite. Estimates of flexural strength of 2D woven SiC/SiC composite are extracted from symmetric and asymmetric 3-point bending test results using three independent approaches: (1) the equations of elastic beam theory for homogneous solids, (2) finite element analysis of stress-state, (3) stress-strain relations in the tensile outer surface of specimens. Furthermore, the flexural strength is predicted from the ultimate tensile strength using a bundle failure model based on the fracture of the critical filament. It is shown that the equation of elastic beam theory significantly overestimates the flexural strength of the 2D SiC/SiC (620 MPa), while the alternate approaches, and the predictions from the ultimate tensile strength converged on ≈340 MPa. The variability of strength data was approached using the construction of p-quantile diagrams that provide unbiased assessment of the normal distribution function. Pertinent Weibull parameters are derived using the 1st moment equations. Important trends in the effects of size, stress gradient, tension-flexure relations, strength of critical filament in a tow and populations of critical flaws are established and discussed.

Keywords: ceramic matrix composites; fiber; strength; tows; fracture; normal distribution; Weibull

1-. Introduction

Composites materials are critical in many applications, and they can replace metallic materials in many systems or goods. The potential applications of ceramic matrix composites reinforced with long continuous ceramic fibers range from room temperature to very high temperature, in ambient or severe environments [1]. The large variety of possible combinations of matrix and fiber types allows the design of composite materials tailored to application requirements and performances. The composite engineering provides materials with properties superior to the properties of constituents considered separately. Fiber reinforced composites are heterogeneous and anisotropic materials. Taking into account the respective contribution of constituents (fibers, matrix, flaws and interfaces) in the mechanical behavior requires multiscale approach-based analyses [2]. Questions relative to proper characterization and safe prediction of the mechanical behavior and the failure of composite components are still open.

Tensile testing is a simple and fundamental materials science and engineering test that provides directly mechanical characteristics of materials. However, some extrinsic difficulties may arise from specimen gripping, alignment and material high cost. Therefore certain authors recommended the flexural test during the development stage of a ceramic-fiber composite system, arguing that it can be carried out on small easily prepared specimens using simple jigs [3]. Authors were also interested in flexural testing with a view to predicting ultimate tensile strength. But, material-induced intrinsic difficulties arise such as the calculation of the flexural strength from the experimental force data, the damage prior to ultimate failure and the influence of stress gradient, specimen size and fabric orientation on the mechanical behavior.

 doi:10.20944/preprints202504.2272.v1

In tensile specimens, during uniaxial tension, a uniform stress-state operates at macroscopic level, and diffuse matrix cracking occurs prior to ultimate failure from a critical fiber [4]. The following mechanisms during flexural tests on relatively long thin specimens were described [5] : « First, multiple cracking occurs on the tensile surface at the same stress as in the tension test. Following matrix cracking, the neutral axis of the beam shifts toward the compressive surface. The compressive stresses are enlarged whereas the tensile stresses are relaxed compared to the stresses in the uncracked beam. After further loading, the peak load is dictated by damage in the compressive side of the beam, and involves fiber buckling and matrix fragmentation ». A numerical analysis of the flexural behavior of a laminated ceramic matrix composite considering the constitutive tensile-compressive behavior of each layer and the constitutive shear behavior of the interlaminar regions showed that the neutral axis of the flexure beam migrates towards the compressive side due to progressive fiber failure in the tensile layers [6]. Delamination cracks were observed on Nicalon SiC/Al_2O_3 [7], and in both transverse and edge-on orientations on Nextel /SiC [8], and in transverse orientation on Nicalon /SiC [8] leading to specimen collapse rather than separation. By contrast, specimen fracture in two pieces was observed on Nicalon /SiC composites in edge-on orientation [8,9] (the SiC matrix of which is twice as stiff as the Nicalon fibers), The load was reported to be transferred equally between the plies [8].

Several values of ultimate flexural strength (UFS) have been reported in the literature for various composites including C/C-SiC [10], Nicalon/C, Nicalon/CAS, Nicalon/LAS [12], Nicalon/SiC [5,8,9,13–15], Nextel/SiC [8], Carbon-reinforced Borosilicate glass [16].

The UFS were found larger than the UTS (Ultimate Tensile Strength). Certain authors attributed this trend to the shift of the neutral axis [7]. Using an experimental and numerical approach [10] it was shown that the trend is partially explained by the differing tensile and compression stress-strain behaviors and further by the work of fracture beyond maximum load. In [[11] the higher the strength ratio was observed when the more the load-deflection curve deviated from linearity. The strength ratio depended most strongly on the behavior of the uniaxial stress-strain curve after the ultimate tensile strength; materials that failed gracefully tended to exhibit higher strength ratio.

The UFS/UTS ratio displayed variability, and depended on the method of determination of flexural strengths. Values of UFS/UTS < 1.5 were obtained using micromechanics based approaches [12,13]. Quite larger ratios (>3) and larger UFS were obtained when the flexural strength was calculated using the simple elastic beam equation [3, 8, 9, 14, 15, 17, 18]. In [6] it was shown that ordinary beam equations cannot be used to describe the behavior. These equations led to the following high values of the flexural strength of Nicalon/SiC:

- in transverse configuration : 320 MPa [8,9], 350 MPa [5,15]
- in edge-on configuration : 500 MPa [9], 430 MPa [8],
- on 3D fabric reinforced composite: 514 MPa [14].

Smaller values were obtained using micromechanics based approach on in edge-on configuration: 213 & 187 MPa, (UFS/UTS ratio ~ 1.26) were obtained from only two tensile tests and two four-point flexure tests [13]. Additionally, it is worth mentioning that composite Weibull modulus of ~ 15 was derived from these experimental data through Monte Carlo simulations [13]. The authors recognized that a large number of tests is needed to ascertain composite Weibull modulus accurately.

It was observed that the UFS of the Nicalon/Al2O3 and the Nicalon/SiC composites calculated using *ordinary beam equations* was not noticeably affected by specimen length increase [8] whereas there was a significant increase in the UFS of Nicalon/SiC composite when the specimen width was increased [8].

Tension-bending relations are required for predicting the tensile strength from the flexural strength, or vice-cersa. The bending moment and neutral axis shifting were introduced in models that did not include the physics-based damage phenomena and required asumptions on the stress profile in the bending specimens [11,13,17,19]. The tensile behavior derived from the bending curve, showed qualitative but not satisfactory agreement with the experimental tensile behavior. The experimental

 doi:10.20944/preprints202504.2272.v1

data base was scarce, and not statistically significant [11,13,17]. A few authors recognized the contribution of fiber to flexural ultimate fracture [12,13,20]. The Foster's analysis [20] related the nominal bend strength of Titanium/SiC Metal Matrix Composite to fiber bundle strength and to matrix yield strength, and used a Local Load Sharing simulation model to study the evolution of fiber damage.

In most cases, the vicious circle in the analysis of flexural strength data was not broken. Which means that models of flexural behavior could not be compared to experimental behavior, due to the lack of an accepted equation for the calculation of empirical flexural stresses from experimental forces. In comparison, this exercise is straightforward for tensile strengths that are calculated from experimental forces using a simple and accepted equation. An attempt to overcome this difficulty is proposed in the present paper by using three different and independent approaches for the determination of flexural strength : (1) finite element analysis of stress-state, (2) fiber bundle- based approach, (3) stress-strain Hooke relation. The simple equation of elastic beam theory was also used for evaluation purpose.

The present paper investigates the flexural strength of CVI 2D woven SiC/SiC composite with respect to avalable tensile strength results [4]. It proposes a multiscale approach that recognizes the underlying contribution to failure of fiber tows, single filaments and the critical filament in a tow after matrix damage. The variability of strength data is characterized using the construction of p-quantile diagrams and the Weibull approach. An exact relation between tensile and flexural strengths is proposed. Important trends in the effects of size, stress gradient, tension-flexure relations, strength of critical filament in a tow and populations of critical flaws are established and discussed

2. Background : The Ultimate Failure Under Tensile Loading Parallel to a Fiber Direction

During tensile tests parallel to a principal fiber direction, ceramic matrix composites exhibit a response depending on the respective Young's moduli of fibers and matrix. Those composites like the SiC/SiC with high matrix modulus and quite strong fiber/matrix interfaces display non linear deformations that result from transverse cracking in the matrix (the cracks are perpendicular to fibres in the loading direction) and limited fiber/matrix debonding. Saturation of matrix damage is indicated by a point of inflection at about 0.4% strain for those composites with a weak interphase, whereas it occurs at higher stress on those composites with a strengthened fibre/matrix interphase. Figure 1 shows the correlative decrease of composite elastic modulus that reflects the increasing damage and the decreasing load carrying capacity of the matrix [2]. The load is transferred to longitudinal tows that carry the whole load after matrix cracking saturation. The analysis of acoustic emission signals indicate that fracture of filaments starts at strains > 0.6%. The composite elastic modulus reaches the minimum dictated by the debonded longitudinal filaments according to the following rule of mixture:

$$E_{min} = E_f V_f \quad (1)$$

V_f is the volume fraction of fibres oriented in the loading direction, E_f is fibre elastic modulus.

It was established [4] that the ultimate failure of composite under *strain-controlled* condition of tensile loading is caused by an overload resulting from the friction of pull-out broken fibres against matrix and transferred evenly to the surviving fibers. The overload increases steadily with the number of broken fibers so that the reinforcing tows are subjected to a *force-controlled* process although *constant strain rate* is applied. The critical fiber which initiates the instability is that when the overload exceeds the filament strength gradient in a tow. The closed form equations that were established for the criterion of initiation and propagation of filament failure in a tow led to a closed form equation for tow and composite strength. The theoretical strength of the critical filament is defined by its rank in the cumulative distribution of filament strengths in a tow, and by the maximum on the tow force-strain curve. The following exact equation of the theoretical strength $_f(P= _c)$, was found to lead to satisfactory predictions of composite tensile ultimate strength [4]:

 doi:10.20944/preprints202504.2272.v1

$$\sigma_f(P=\alpha_c)=\sigma_0\left[\frac{V_0}{V}\frac{1}{m}\right]^{\frac{1}{m}}=\mu\frac{m^{-1/m}}{\Gamma\left(1+\frac{1}{m}\right)} \quad (2)$$

where P is failure probability, α_c is failure probability the critical filament strength, m and σ_0 are the Weibull statistical parameters pertinent to filament strengths, V is the volume, V is the reference volume (1m²), is the mean stress, Γ is the gamma function,

Equation (2) was found to be more appropriate than equations proposed in the literature that misestimated significantly the strength [4]. It is worth pointing out that equation (2) shows that the theoretical strength $\sigma_f(P=\alpha_c)$ takes a unique value when statistical parameters are invariant with tow specimens of identical dimensions [4,21]. However, experimental results show that the rank and the strength of critical flament are affected by structural effects like local friction. The associated strength scatter was attributed to the variation in friction induced overload resulting from variability in fiber/matrix interface characteristics and filament surface roughness.

Under these conditions of strain-controlled loading, and in the absence of pull-out friction from broken fibers, the fracture would be dictated by the strength of the strongest filament. The force-strain curve would exhibit a smooth and stable force decrease.

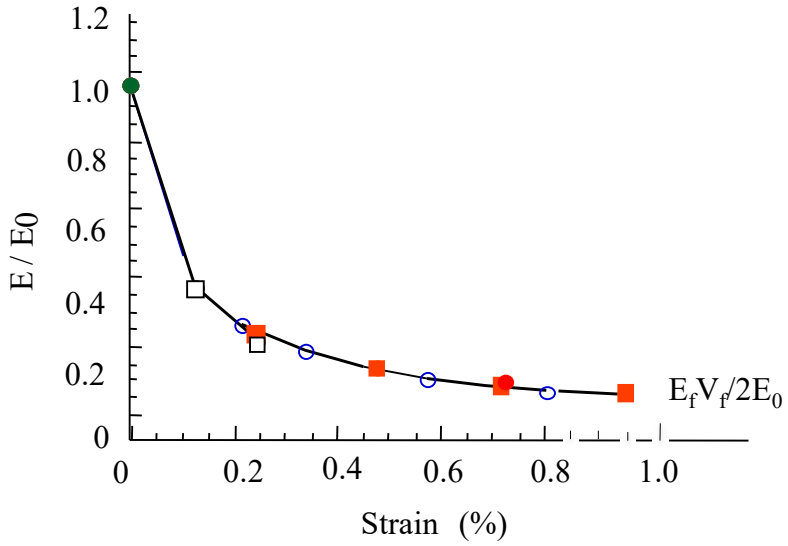

Figure 1. Relative elastic modulus versus strain during tensile tests on 2D woven SiC/SiC composite [1,2].

3. Experimental : Material and Procedure

The experimental results were generated in a previous paper [22,23]. The 3-point bending tests were performed on 2D woven SiC/SiC composite specimens made via chemical vapor infiltration (CVI) [22,23]. SiC/SiC was reinforced by about f SiC Nicalon fibres in a plain weave configuration. The testspecimens were cut out of plates 3.3 mm thick. Two batches of straight bars (8x80x3.3 mm³) for the symmetric and asymmetric 3-pt bending tests that generate symmetric and asymmetric stress gradients.

The flexural specimens were loaded edge-on parallel to the woven plies, in order to prevent delamination between layers and thus, compare properly tension and bending results. Furthermore, the specimens were relatively thin (height/span length = 0.1) so that the relative shear stress was minimized. The displacement rate was chosen so as to obtain the same strain rate of 4 10^{-4} %/s in the outer tensile face as for the tensile testspecimens. Strains in the outer tensile face were measured using an extensometer with a 10 mm gauge length (Figure 2a).

 doi:10.20944/preprints202504.2272.v1

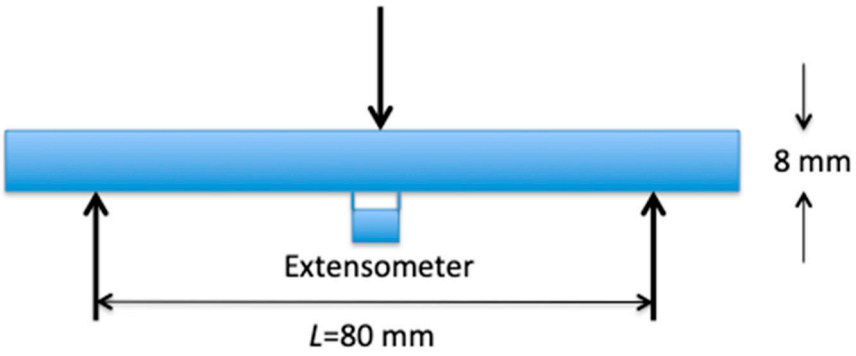

(a)

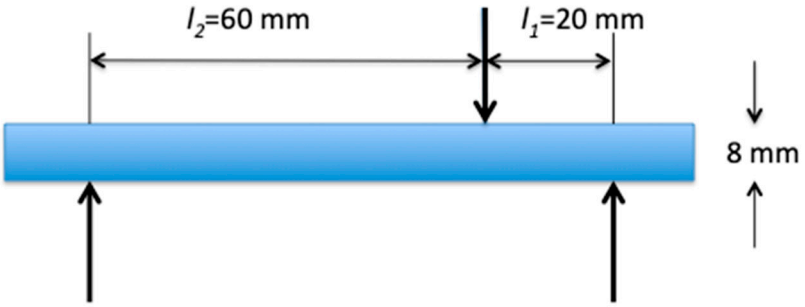

(b)

Figure 2. The 3-point bending tests : (a) symmetric, (b) asymmetric tests.

The experimental results of tensile tests were reported in a previous paper. The two batches of each 12 tensile SiC/SiC specimens were manufactured together with the batches of bending specimens: a batch of small (V_1= 8x30x3.3 mm^3) and a batch of large (V_2 = 16x120x3.3 mm^3) dogbone shaped-specimens [22,23]. The flexural and the smaller tensile specimens had identical cross-section dimensions. The strain rate was 4 10^{-4} %. Strains were measured using an extensometer over a 25 mm gauge length

4. Determination of Flexural Strength

4.1- Finite Element Analysis

A mesh of 4x40 quadrilateral elements (size : 2x2 mm^2) was constructed for the finite element analysis of the stress-state [11]. The size of elements was selected according to that of Representative Volume Element. The boundary conditions reproduced the loading conditions in the 3-pt bending tests as described above : (i) displacements applied through the upper roller, (ii) plane stress conditions. The compressive behaviour was taken to be linear although a slight non linearity has been reported by McNulty and Zok [5]. The contribution of damage to deformations in the tensile part of specimens was taken into account using the Young's modulus-strain relationship determined from the strain-stress behaviour obtained during tensile tests [1,2] (figure 2). For this purpose, strains were computed first for the initial value of composite Young's modulus (226 GPa: table 1). Then, for the same applied displacement, they were computed for values of Young's

 doi:10.20944/preprints202504.2272.v1

modulus corresponding to the current strain-state. The procedure was iterated until the discrepancy between strains at two successive steps was negligible. The tensile response was assumed to be orthotropic, with non coupled tow directions. Since the specimens were loaded parallel to the plies, the transverse properties were neglected.

The finite element computations provided the strain- and stress-fields for various applied forces. The force-strain curves relate the applied forces and the corresponding strains located in the outer face on the force axis. The ultimate strength is given by the maximum tensile stress computed for the failure force measured during the tests.

4.2- Elastic beam theory

The flexural strength under symmetric 3-point bending was alternately derived using the following formulae based on the elastic beam theory for homogeneous isotropic solid:

$$\boldsymbol{\sigma_f = \frac{3F_m L}{2bh^2}} (3)$$

where F_m is the maximum applied force; L is the outer span length, b is the mean width and h is the mean thickness of the test specimen.

This equation is based on the following assmptions:

- The beam is symmetrical about neutral plane
- The beam is a straight bar of homogeneous and linearly elastic material
- The transverse plane sections remain plane and normal to the longitudinal fibres after bending (Bernoulli's assumption).
- The fixed relationship between stress and strain (Young's modulus) for the beam material is the same for tension and compression.

The behavior of beams made of CFRC composites is different from that of homogeneous elastic materials as soon as matrix damage initiates. This equation was used although its applicability to fiber-reinforced CMC is questionned, in order to evaluate error on estimated strength.

4.3. Strength estimated from measured strain at failure

The flexural strength is related to the maximum strain at failure in the outer tensile surface of bending specimen by the Hooke equation:

$$\boldsymbol{\sigma_{flex} = E(\varepsilon_{max})\varepsilon_{max} = E_f V_f \varepsilon_{max}} (4)$$

where ε_{max} is the maximum strain in the outer surface of specimens, and $E(\varepsilon_{max})$ is the corresponding value of Young's modulus, which was derived from tensile tests, after saturation of matrix cracking [1]: $E(\varepsilon_{max}) = E_{min}$ is given by equation (1). E_f is the Young's modulus of filaments, V_f is the fraction of fibers in the longitudinal axis direction. Assuming a linear strain gradient, ε_{max} was derived from the measured strain $\varepsilon_{measured}$ using the following equation:

$$\boldsymbol{\varepsilon_{max} = \frac{L}{L-2z}\varepsilon(z)} (5)$$

where z is the abscissa of $\varepsilon(z)$ on longitudinal axis of specimen, z=0 for ε_{max} at midspan, z=5 mm for $\varepsilon_{measured}$ (half gage length). L is the span length. The flexural strength was calculated using equations (4) and (5) for the SiC/SiC experimental data given in Table 1.

Table 1. Values of experimental data used for the determination of the flexural strength.

E_0 GPa	E_f GPa	V_f	$\varepsilon_{measured}$ %	ε_{max} %	L mm	Filament Weibull modulus
226	200	0.18	0.8	0.91	80	5.3

4.4. Prediction: The Bundle-Based Approach

It was assumed that the critical tow is completely debonded after saturation of matrix cracking, which is also supported by several results [1,2]. It was assumed that failure due to shear is not an issue and our concern is the longitudinal direction stress and its resulting distribution. The fibers are

 doi:10.20944/preprints202504.2272.v1

subjected to a bending moment, which generates a stress gradient. The principle of the approach is to define a volume equivalent to the fiber stressed volume under uniform tension on the basis of Weibull statistics, and then to derive the bending strength from the tensile strength for the critical fiber in the tow. It has been shown that multifilament tows are elastic and damage tolerant, whereas single fibers are brittle. The multifilament tows exhibit a non-linear force-strain relation resulting from successive individual fiber breaks under controlled deformation rate [21]. The fraction of fiber fractures at maximum force defines the critical filament that can initiate the failure of tow [21]. It is widely accepted that the Weibull model satisfactorily describes the statistical distribution of failure strengths of single filaments under tensile loads [24].

Symmetric 3-point bending

The approach is founded on the following asumptions :

- A tensile tress gradient operated along specimen length
- The stress was considered to be constant through the cross section of filaments in the tensile part of beam. The through thickness stress gradient can be neglected because fiber diameter (12 micrometers) is negligible compared to specimen thickness (4 mm in the tensile part).
- The highest stresses operated on the extreme ply close to the specimen outer surface under tension.
- As discussed in previous papers, fracture is initiated from a critical fiber in the ply subjected to highest tensile longitudinal stresses, after saturation of matrix cracking.
- A linear tensile stress gradient on filaments located at the bottom side of the beam was assumed. It is symmetric with respect to the loading axis:

$$\sigma = \sigma_{max}\left(1 - \frac{2z}{L}\right) \quad (6)$$

where σ_{max} is the peak tensile stress in the ply. L is the span length. The origin is the center of the specimen, $-L/2<z<L/2$, L is the stressed fiber length.

The volume of a statistically equivalent ply subjected to peak tensile stress operating uniformly was defined using the cumulative Weibull distribution of filament strengths σ [25]:

$$\boldsymbol{P = 1 - exp\left[-\int_{-L/2}^{L/2} \frac{1}{V_0}\left(\frac{\sigma}{\sigma_0}\right)^m S dz\right]} \quad (7)$$

where σ_0 is the scale factor, m is the Weibull modulus, S is the cross sectional area of a filament, V_0 is a reference volume (V_0=1m^3).

Introducing equation (6) into (7), and integrating it comes :

$$\boldsymbol{P = 1 - exp\left[-\frac{LS}{m+1}\frac{1}{V_0}\left(\frac{\sigma_{max}}{\sigma_0}\right)^m\right]} \quad (8)$$

Equation (9) gives the equivalent filament stressed volume subjected to σ_{max} operating uniformly:

$$\boldsymbol{V_{eq} = \frac{LS}{m+1}} \quad (9)$$

The cumulative distribution of filament strengths under uniform tension is:

$$\boldsymbol{P = 1 - exp\left[-l_t S \frac{1}{V_0}\left(\frac{\sigma_t}{\sigma_0}\right)^m\right]} \quad (10)$$

where σ_t is fiber tensile strength, l_t is the gauge length.

The relation between the bending and the tensile filament strengths is obtained from equating probabilities:

$$\boldsymbol{\sigma_{max} = \sigma_t\left[\frac{l_t}{L}(m_c + 1)\right]^{\frac{1}{m_c}}} \quad (11)$$

For the volume fraction of longitudinal fibers V_f, the flexural strength of composite is related to the strength of tensile specimen by the expression:

 doi:10.20944/preprints202504.2272.v1

$$\boldsymbol{\sigma_{flex} = \sigma_{tr}\left[\frac{l_t}{L}(m_c + 1)\right]^{\frac{1}{m_c}}}(12)$$

$\boldsymbol{\sigma_{flex} = V_f \sigma^c_{max}}$ and $\boldsymbol{\sigma_{tr} = V_f \sigma^c_t}$. σ_{flex}. σ_{flex} is composite flexural strength, $\boldsymbol{\sigma^c_{max}}$ is the strength of critical filament in flexural specimen, σ_{tr} is the strength of tensile specimen, $\boldsymbol{\sigma^c_t}$ is the tensile strength of the critical fiber in the tensile specimen having gauge length l_t. m_c is the Weibull modulus of critical filament strength.

It is important to point out that equations (7) to (10) are relative to filament distribution, whereas equations (11) and (12) derive from equations relative to filaments having the same specified probability. Equation (12) corresponds to the critical filament that fails in critical tow at fracture of a tensile or flexural composite testspecimen: $\boldsymbol{\sigma^c_t = \sigma^c_{max} = \sigma_t(P = \alpha_c)}$. $\sigma_t(P=\alpha_c)$ is given by equation (2).

Asymmetric 3-point bending

The approach is founded on the same asumptions as above. The following asymmetric linear tensile stress gradient on fibers located at the bottom side of the beam was assumed:

$$\boldsymbol{\sigma = \sigma_{max}\left(1 - \frac{z}{l_1}\right)} 0<z<l_1 (13)$$

$$\boldsymbol{\sigma = \sigma_{max}\left(1 - \frac{z}{l_2}\right)} 0>z>-l_2 (14)$$

The origin is located on the loading axis, $-l_2<z<l_1$, with $l_2+l_1=L$. l_2 and l_1 are defined on figure 2.
The probability of failure of a filament under stress σ, is given by:

$$\boldsymbol{P = 1 - exp\left[-\int_{-l_2}^{l_1} \frac{1}{V_0}\left(\frac{\sigma}{\sigma_0}\right)^m Sdz\right]}(15)$$

Introducing equations (13) and (14) into (15) and integrating it comes :

$$\boldsymbol{P = 1 - exp\left[-\frac{LS}{m+1}\frac{1}{V_0}\left(\frac{\sigma_{max}}{\sigma_0}\right)^m\right]}(16)$$

The effective volume defined by equation (16) is given by the same equation as above for symmetric bending: $\boldsymbol{V_{eq} = \frac{LS}{m+1}}$. As a consequence, the flexural strength is given also by equation (12), which indicates that is not affected by asymmetric stress gradient.

5. Strength Variability

Strength variability was approached using p-quantile diagrams that provide a proper and unbiased way to evaluate the pertinence of normal distribution function. Thus, it was demonstrated that when the plot of the p-quantile z_p vs. strength σ_p is linear, it can be concluded that the strength is a Gaussian variable [24].

The equation of p-quantile diagrams is:

$$\boldsymbol{z_p = \Phi^{-1}(P) = \frac{\sigma_p - \mu}{s}}(17)$$

where $P=i/(n+1)$, μ = mean, s = standard deviation, σ_p is the value of strength with probability P, and Φ is the cumulative standard normal distribution of variable z.

$$\boldsymbol{\Phi(z) = \frac{1}{s\sqrt{2\pi}}\int_0^z \exp\left(-\frac{(t-\mu)^2}{2s^2}\right) dt}(18)$$

The normal cumulative distribution function (CDF) was calculated using Equation (18) for the values of the mean μ and standard deviation s of the sets of experimental strength data.

The Weibull parameters were derived from μ and s, using the 1st moment equations:

$$\boldsymbol{\frac{s}{\mu} = \sqrt{\left[\frac{\Gamma\left(1+\frac{2}{m}\right)}{\Gamma^2\left(1+\frac{1}{m}\right)} - 1\right]} \cong \frac{1.2}{m}}(19)$$

$$\boldsymbol{\sigma_l = \frac{\mu}{\Gamma\left(1+\frac{1}{m}\right)}}(20)$$

 doi:10.20944/preprints202504.2272.v1

where σ_l is the characteristic strength.The Weibull cumulative distribution function was calculated using the following equation:

$$P_w(\Sigma < \sigma) = 1 - \exp\left[-\left(\frac{\sigma}{\sigma_l}\right)^m\right] \text{ for } \sigma > 0 \quad (21)$$

The Weibull function was then validated by comparing the CDF to the reference normal distribution of experimental strength data.

6. Results

6.1. The Stress-Strain Curve

Ultimate failure was characterized by specimen fracture into two pieces. It occurred systematically under the loading points from the outer surface of beams, at the expected location of maximum tensile stress. The force-strain curves exhibited non-linear deformations at strains increasing from values < 0.1% (figure 3), like the behavior in traction [4]. Which reflects matrix cracking and associated interface debonding. The strains at maximum forces were of the same order of magnitude as the strains-to-failure of fibers tows (0.8%) [26]. Figure 3 shows that the computed force-strain curve reproduces well the experimental flexure behavior which validates the finite element analysis of strains and stresses. Note that the experimental behavior is plotted with respect to force values since a reference stress-strain curve cannot be extracted from force data because well-accepted exact equations of stresses are not available.

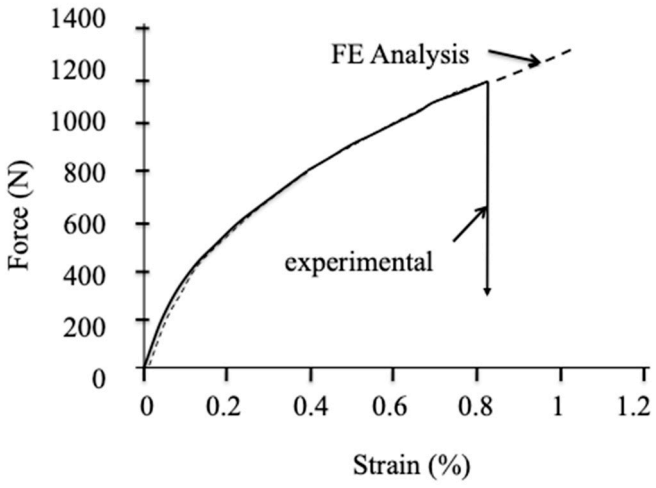

Figure 3. Example of force stress-strain curve obtained experimentally using symmetric 3-point bending tests. Comparison with computed flexure behavior.

6.2. Flexural Ultimate Strengths

Table 2 and figure 4 compare the flexural strengths determined using the different approaches. All the approaches provided flexural strength magnitudes that exceed the tensile strength value (Table 2, figure 4). They converge consistently to a value of about 340 MPa, unlike the equation of elastic beam theory that estimated the value to be very nearly double. The flexural strengths predicted from tensile strength (equation (12)) compare quite well with the results of Finite Element Analysis and the values derived from failure strains.

Table 2. Average estimates of flexural ultimate strengths, and predictions using the equation (12) of bundle model. Also reported is the tensile strength.

	Strength (MPa)	Ratio $\sigma_{flex}/\sigma_{traction}$
Traction	300	

 doi:10.20944/preprints202504.2272.v1

3-pt symmetric EBT equations	619	2.06
3-pt symmetric FE Analysis	341	1.14
3-pt symmetric Measured Strain (MPa)	327	1.09
3-pt asymmetric FE Analysis (MPa)	350	1.17
3-pt prediction equation (12) (from traction V_1)	335	1.11
3-pt prediction equation (12) (from traction V_2)	353	1.17

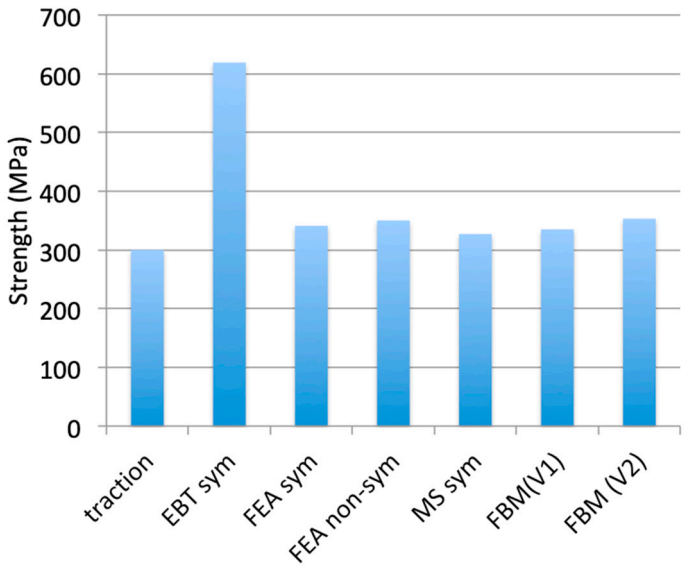

Figure 4. Average values of flexural strengths determined using various methods: EBT (Elastic Beam Theory), FEA (Finite Element Analysis), MS (Measured Strain), FBM (Fiber Bundle Model). Also plotted is the strength measured using tensile test (traction).

6.3. Strength Variability

Figure 5 shows that the plots of *p*-quantiles versus strengths fit straight lines. The goodness of fit is characterized by high values of coefficients of linear regression ($R^2 > 0.96$) (Table 3). It can be inferred from these results that the flexural strength distributions can be approximated by the normal distribution function. The plots indicate clearly the respective means (for $z_p = 0$) and the magnitude of dispersion of strength data (by the slope = 1/s). The statistical parameters of normal and Weibull distribution functions are given in table 4.

The p-quantile diagrams of FEA flexural strengths were distinct from the tensile ones, indicating a small dependence on dimensions and stress-state (figure 5). Figure 5 shows also the p-quantile diagrams of flexural strengths predicted from tensile strengths using equation (12) for the m_c estimates given in table 4, and the current gauge lengths of tensile specimens (l_t) and span lengh (L). The predictions agree satisfactorily with the FEA flexural strengths.

The p-quantile diagrams of tensile strengths were superposed, indicating that the tensile strength was independent of specimen dimensions. As mentioned above, the results based on the equation of Elastic Beam Theory looked overestimated.

 doi:10.20944/preprints202504.2272.v1

The p-quantile vs strains-to-failure diagrams displayed a small dependence on the size of equivalent stressed volume (Figure 6).

Figure 7 shows that the Weibull distributions of strengths fit the normal distributions. The goodness of fit is confirmed by the high values of coefficents of corrrelation R2 (Table 3). Visually it is less satisfactory for the strengths data estimated using the equation of elastic beam theory. Since the validity of normal distribution was assessed by the linearity of p-quantile diagrams, it can be inferred that the strength data follow Weibull distribution function. However, it is worth pointing out that the Weibull parameters were not constant, which implies that the Weibull equation was not unique.

Table 3. Coefficients of correlation relative to p-quantiles-strengths diagrams, and normal vs Weibull CDF.

	p-quantile vs strengths	normal vs Weibull
Traction V1	0.96	0.98
Traction V2	0.97	0.98
3pt symmetric FEA	0.98	0.99
3pt nonsymmetric FEA	0.97	0.99
3pt symmetric EBT	0.99	0.97

Table 4. Statistical parameters of composite strength distributions.

	μ MPa)	s (MPa)	m_c	σ_l (MPa)
Traction V1	300	20.74	17.3	313.8
Traction V2	294	19.24	18.35	306.6
3pt symmetric FEA	340.18	9.8	41.69	344.66
3pt nonsymmetric FEA	350.34	11.09	37.9	355.67
3pt symmetric EBT	600	22.22	32.42	629.63

6.4 Critical Filament

The strengths of critical filaments were derived from the composite strengths (σ_{comp}) using the following commonly accepted equation:

$$\boldsymbol{\sigma_f} = \frac{\boldsymbol{\sigma_{comp}}}{\boldsymbol{V_f}} \quad (22)$$

Figure 8 compares the strengths of critical filaments in composite (σ_f) given by equation (22) to the strengths of filaments extracted from the typical force-strain curve of SiC Nicalon tows displayed in [26]. It is worth pointing out that the estimated values of σ_ϕ were close to the theoretical strength of critical filament in the tow defined by σ ($P=\alpha_c$) (equation (2)), which is consistent with the analysis. By contrast, the results from EBT were close to the high extreme of filament strength distribution, which corresponds to values of strains around 1.7%. Such strain magnitudes are not consistent with the experimental composite strains at ultimate failure (around 0.9%).

 doi:10.20944/preprints202504.2272.v1

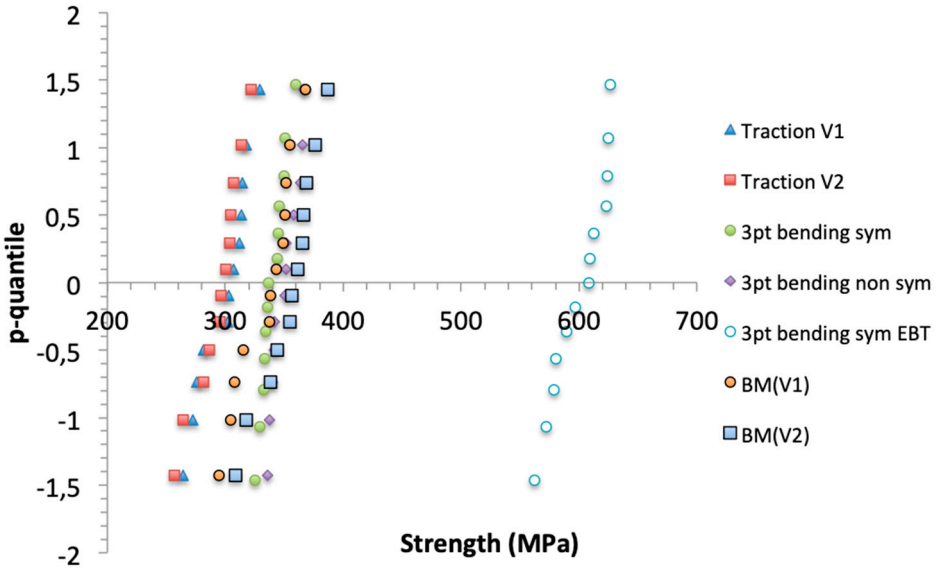

Figure 5. Plots of p-quantiles vs. strengths in traction and in bending. BM(V1) and BM(V2) refer to strengths predicted using bundle model from tensile strengths of specimens having volume V1 or V2.

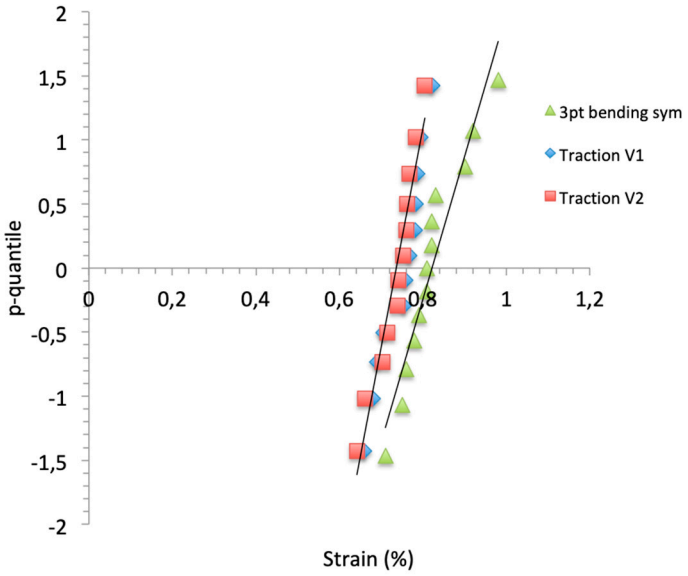

Figure 6. Plots of p-quantile vs. strains-to-failure.

 doi:10.20944/preprints202504.2272.v1

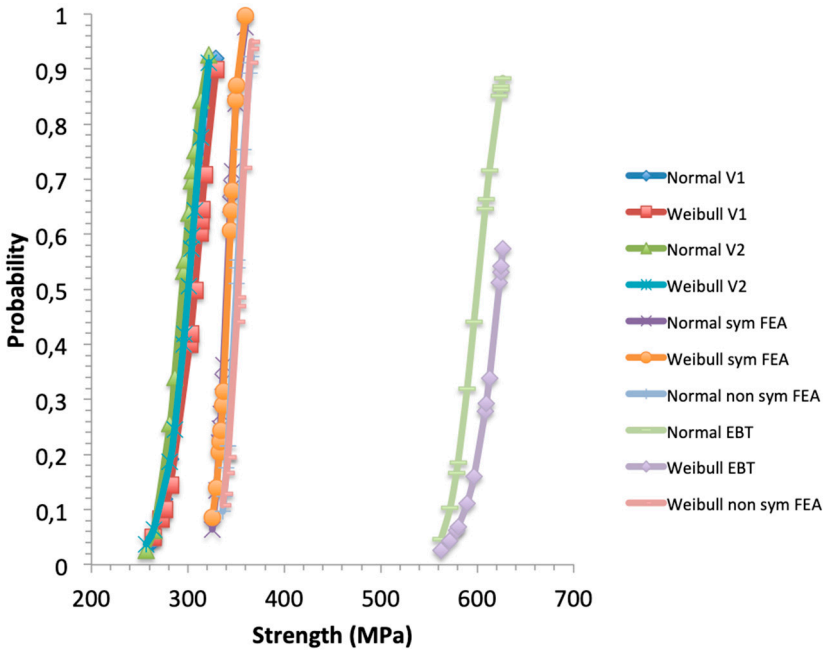

Figure 7. Normal and Weibull cumulative distributions of traction (referred to as Normal V_1 or V_2, Weibull V_1 or V_2), and flexural strengths.

7. Discussion

7.1. Flexural Strength

The elastic beam theory-based equation provided significantly overestimated flexural strengths when comparing with the values obtained using the alternative approaches. This trend was confirmed by the corresponding ratio of flexural-to-tensile strengths (table 2) that was > 2. A similar strength ratio was obtained with the EBT equation on a first generation of SiC/SiC with low strain-to-failure (< 0.2%) and on C/SiC [27]. Such high ratios suggest that the composites are as sensitive to flaws as monolithic ceramics [17], on which the strength ratio is 2 for $m \approx 6$ [28]. Such degree of sensitiity looks paradoxical since composite tensile strengths were found to be independent of specimen dimensions, and large values of composite Weibull modulus (m_c>18 ; table 2) were observed in this paper. The flexural/tensile strength ratios obtained with the three alternative approaches are around 1.15 (table 2). The value of 1.26 was reported in [13]. Values of 1.4-1.5 were obtained on glass-fiber-reinforced polymers in [29,30]. These results contradict the following trend stated by several authors that « the flexural strength can exceed the tensile strength by a factor of 3 » [11,17,19].

By analogy with the tensile behavior under strain controlled conditions, it is reasonable to consider that the flexural strength of composites results from overloading by local friction due to distributive pull out of broken fibers, owing to the tensile stress-state operating parallel to longitudinal fiber axis. Furthermore, more fibers are increasingly subjected to tensile stresses as the neutral axis of the beam shifts toward the compressive surface. It is important to remind that the loading mode was strain- controlled in both the tensile and flexural tests, so that the resulting stress operating on a fiber before failure was not transferred on the surviving fibers [31]. Therefore, the scatter of experimental strengths of critical filaments was logically attributed to variability in interface characteristics and fibre surface roughness. Furthermore, it is worth pointing out that the high strength extreme in the distribution of filament critical strengths coincided with the theoretical value (figure 8).

The linearity of p-quantile diagrams seems to be acceptable, which means that the strength distributions can be approximated by normal distribution functions. The Weibull CDF showed good agreement with the corresponding normal distributions. The tensile strength distributions did not display dependence on tensile specimen dimensions, which can be attributed to the fact that the flaw

 doi:10.20944/preprints202504.2272.v1

populations were reproducible, in other words that each tensile specimen contained the full population of flaws inherent to the considered fiber type. This results from the huge number of critical flaws/filaments in a tensile composite test specimen that contains roughly 30000 filaments as pointed out in a previous paper [4]. The statistical parameters of composite tensile strengths were quite close. From this feature, it can be inferred that the tensile strength data can be characterized by unique normal and Weibull distribution functions.

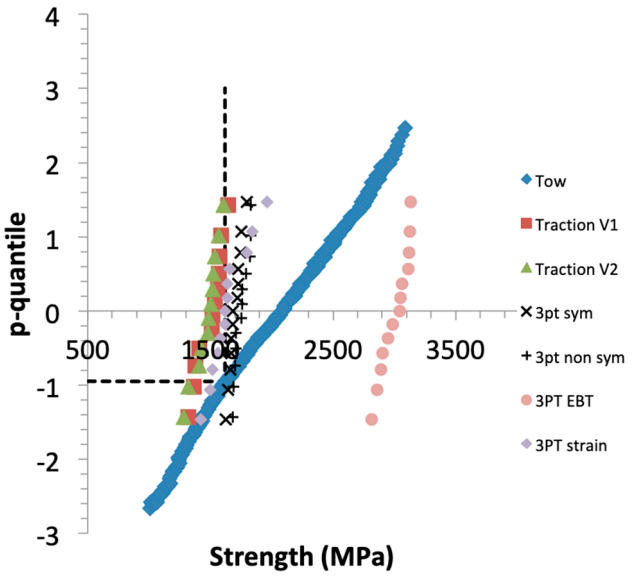

Figure 8. Plot of filament strengths derived from a tow test, and filament strengths derived from composite strengths. Also indicated (dotted line) is the theoretical strength of a tow under loading at a constant stressing rate $\sigma_f(P=\alpha_c)$.

The flexural strength statistical parameters were significantly different from the tensile strength ones. This feature can be attributed to the stress gradient that induces an equivalent stressed volume much smaller than that of tensile specimens. According to equation (9) of equivalent volume, the equivalent gauge length was 13 mm. It is significantly smaller than the critical size above which the full population of critical flaws is present. This critical size was shown to be around 60 mm for SiC fiber tows [32]. Therefore, the population of critical flaws in the tensile stressed volume of flexural specimens probably differed from the full population. It was less heterogeneous and the strengths of critical filaments were larger in the CDF, as big flaws are less frequently present in small volumes. This effect is reflected by the increase in Weibull parameters. It can be simulated by truncating strength distribution.

Nevertheless, the bundle model (equation (12)) predicted flexural strengths that compared well with the experimental strengths, although the Weibull parameters of tensile and flexural specimens were significantly different (figure 5). This goodness of fit results from the limited influence of m_c increases at high values (equation (12)). Figure 9 depicts the variations of the ratio of flexural to tensile strengths as a function of Weibull modulus m_c for various ratios of gauge/span lengths. It shows that the ratio of flexural to traction strengths < 1.2 when $m_c > 10$, and < 1.1 for the current values of m_c: 18 for traction, and 40 for bending. Figure 10 also shows that the influence of m_c becomes significant for $m_c<3$.

7.2. Implications for the Prediction of Tensile Strength from Bending Strength Data

Concerning the prediction of tensile strength from flexural test results, it appears from the above that large flexural test specimens would be preferred in order to impair the size effect. However, the use of large specimens may limit the interest of flexural tests with respect to the practical disadvantages of traction tests on composites. With large testspecimens, the flexural strength may be a good estimate of tensile strength when the specimens contain the full population of critical flaws or when the Weibull modulus m_c is quite large (typically $m_c > 20$).

 doi:10.20944/preprints202504.2272.v1

When small flexural test specimens are used, equation (12) should allow prediction of tensile strength when the Weibull moduli of flexural and tensile strengths do not exhibit significant variation. If any, the difference in Weibull moduli will not affect the predictions when $m_c > 20$.

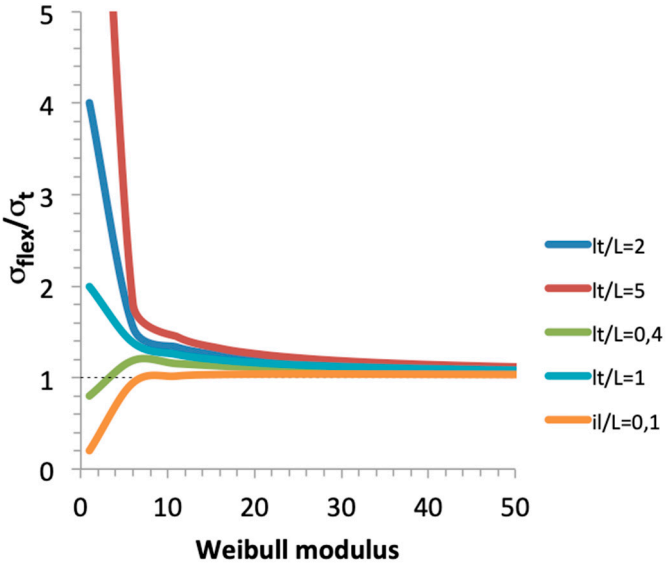

Figure 9. Influence of composite Weibull modulus on ratio of flexural to tensile strengths, for various ratios of gauge/span lengths**.**

7.3. Reproducibility of Flaw Population

Is it reasonable to expect a reproducible flaw population at small gauge lengths below the tow critical size, so that the distribution functions are unique (constant statistical parameters) ? This issue can be examined by considering the relation between the sizes of crack-like critical flaws at increasing volume.

At a given value of probability in the CDF, filament tensile strengths at increasing volume are related by the following equation derived from equation (10), for constant statistical parameters:

$$\frac{\sigma_{2i}}{\sigma_{1i}} = \left(\frac{V_1}{V_2}\right)^{1/m} = \sqrt{\frac{a_{1i}}{a_{2i}}} \quad (30)$$

where σ_{2i} and σ_{1i} are the strengths at volumes $V_2 > V_1$ respectively. a_{2i} and a_{1i} are the corresponding flaw sizes related to strengths by the fracture mechanics equation; i is the rank of strengths in the CDF:

$$\mathbf{K_{IC}} = \boldsymbol{\sigma_i} \mathbf{Y} \sqrt{\mathbf{a_i}} \quad (31)$$

where Y is a constant.

The flaw sizes at constant probability are scaled according to the following equation as the volume increases.

$$\boldsymbol{a_{2i}} = \boldsymbol{a_{i1}} \left(\frac{V_2}{V_1}\right)^{2/m} \quad (32)$$

Equation (32) expresses the requirement that must be met by flaw sizes so that the tensile strength distributions follow the Weibull distribution whatever the dimensions. It can be reasonably conjectured that the probability of this event is very small. Therefore, it seems reasonable to draw the conclusion that, in most cases, the Weibull distribution fonction depends on specimen dimensions below the critical size. Which is an additional disadvantage for the use of small size test specimens.

8. Conclusion

 doi:10.20944/preprints202504.2272.v1

Various original results were obtained in this paper on the flexural strength of fiber reinforced SiC/SiC, on its relation with tensile strength and with the strength of the critical filament that triggers failure of a fiber tow. The determination of flexural strengths of fiber reinforced composites is not straightforward, as the classical equation for homogeneous materials and elastic beams was found to significantly overestimate the SiC/SiC value by a factor of 2. The alternative approaches based on either finite element analysis or strain measurement as well as the predictions from tensile strength led to an estimate close to 340 MPa, slightly larger than the value obtained using tensile tests.

The scatter of flexural strengths was characterized satisfactorily by normal and Weibull distribution functions. It was attributed to the sources of variability identified on tensile tests i.e. the variability in the overloading of filaments governed by fiber/matrix interface characteristics. The strengths were related to scatter of critical filament strength around the theoretical value.

The flexural strengths were slightly larger than the tensile strengths, reflecting a limited specimen size effect. This size effect was attributed to the small equivalent stressed volume of flexural specimens, such that the gauge length was probably below the critical size when the full population of critical flaws is present. The relation between flexural and tensile strengths was satisfactorily predicted using the fiber tow based model. This model appears to be pertinent for those composites which fail from debonded tows after saturation of matrix cracking (which means that they didn't experience premature failure).

From these results it can be anticipated that small flexural test specimens may be not appropriate for estimating tensile strengths, except when the flexural and tensile strengths follow a unique distribution function. A perequisite for this is to assess the validity of distribution functions using an unbiased approach like the p-quantile based method. Then the pertinence of prediction of tensile strengths will depend on the magnitude of Weibull modulus, as the Weibull modulus is expected to exhibit variability below a critical specimen size. Variability at high values will not affect the predictions. Because of these limitations, small flexural specimens cannot be recommended.

Bending tests on damage tolerant CMCs must be regarded as tests on components. A sophisticated analysis is required to derive stress data. By contrast, tensile testing is more appropriate to determine some generic properties that are useful for material evaluation or as input for models.

Funding: This research received no external funding.

Data Availability Statement: Data are available upon request

Conflicts of Interest: The author declares no conflict of interest.

References

1. Lamon, J. CVI SiC/SiC Composites. In *Handbook of Ceramics and Glasses*. Bansal, N.P.,Ed ; Kluwer Academic Publishers, New York, USA, 2005; Chapter 3, pp. 55-76.
2. Lamon, J. Approach to microstructure-behavior relationships for ceramic matrix composites reinforced by continuous fibres. In *Ceramic Matrix Composites: materials, modeling and applications*. Bansal, N.P., Lamon, J., Eds, John Wiley and Sons, Inc., Hoboken, New Jersey, USA, 2014; Chapter 18.
3. Davidge, R.W. The mechanical properties and Fracture behavior of ceramic matrix composites reinforced with continuous fibers. In *Application of fracture mechanics to composite materials*, K. Friedrich, K., Ed; Elsevier Science Publishers, Amsterdam, The Netherlands 1989 ; Volume 6, Chapter 13, pp. 547-569.
4. Lamon, J. The Ultimate Tensile Strength of SiC/SiC Composites: Multiscale Approach. *J. Compos. Sci.* **2025**, *9*, 45. https://doi.org/10.3390/jcs9010045
5. Marshall, D.B.; Ritter, J.E. Reliability of Advanced structural ceramics and ceramic matrix composites. *Ceramic Bulletin* **1987**, *66*, 309-317.
6. Raghuraman, S.; Lara Curzio, E.; Ferber M.K. Modeling of flexural behavior of continuous fiber ceramic composites. *Ceramic Engineering and Science Proceedings* **1996,** *17*, 47 - 156.
7. Miriyala, N.; Liaw, P.K.; McHargue, C.J.; Selvaratinam, A.; Snead, L.L. The effect of fabric orientation on the flexural behavior of CFCCs : experiment and theory. In *Advances in Ceramic Matrix Composites IV*. *Ceramic Transactions*; Singh, J.P., Bansal, N.P., Eds.; 1999, The American Society, Westerville, OH, USA, 1999; 451-463.

 doi:10.20944/preprints202504.2272.v1

8. Chawla, N.; Liaw, P.K.; Lara-Curzio, E.; Ferber, M.K.; Lowden, R.A. Effect of fiber fabric orientation on the flexural monotonic and fatigue behavior of 2D woven ceramic matrix composites, *Materials Science & Engineering A* **2012**, *557*, 77–83.
9. Miriyala, N.; Liaw, P.K.; McHargue, C.J.; Snead, L.L. Specimen size effects on the flexural behavior of CFCCs . *Ceramic Engineering and Science Proceedings* Bray, D., Ed; The American Society, Westerville, OH, 1998; *19*, 3, pp199-209.
10. Hofmann, S.; Öztürk, B.; Koch, D.; Voggenreiter, H. Experimental and numerical evaluation of bending and tensile behaviour of carbon-fibre reinforced SiC. *Composites Part A: Applied Science and Manufacturing* 2012; *43*,
11. Steif, P. S. ; Trojnacki, Bend strength versus tensile strength of fiber-reinforced ceramic composites. *J. Am. Ceram. Soc.*,Vol. **1994**, *77*, pp. 221-229.
12. Hild, F.; Domergue, J.-M.; Leckie, F.A. ; Evans, A.G. Tensile and flexural ultimate strength of fiber-reinforced ceramic-matrix composite. *International Journal of Solids and Structures* **1994**; *31*, *7*, pp. 1035-1045.
13. McNulty, J.C. ; Zok, F.W. Application of weakest-link fracture statistics to fiber-reinforced ceramic-matrix composites. *J. Am. Ceram. Soc.* **1997**, *80*, pp. 1535-43.
14. Chulya, A; Gyekenyesi, J.Z.; Gyekenyesi, J.P. Failure mechanisms of 3-D woven SiC/SiC composites under tensile and flexural loading at room and elevated temperatures. Proceedings of the 16th Annual Conference on Composites and Advanced Ceramic Materials, January, Cocoa Beach, FL, Ceramic Engineering and Science Proceedings; The American Society, Westerville, OH, 1992, pp. 421-432.
15. Caputo, A.J.; Lackey, W.J. ; Stinton, D.P. Development of a New, Faster Process for the Fabrication of Ceramic Fiber- Reinforced Ceramic Composites by Chemical Vapor Infiltration. *Ceram. Eng. & Sci. Proc*.6 **1985**, 694-706.
16. Morrell, R. ; McCartney, L.N. Measurement of properties of brittle matrix composites, *Br. Ceram. Trans*. 1993, *92*, 1-7.
17. Laws, V.Derivation of the tensile stress-strain curve from bending data. *J. Mater. Sci*.**198**1, *16*, pp. 1299-1304.
18. Aveston, J.; Mercer, R. A.; Sillwood, J. M. Composites – Standard Testing and Design, Conference Proceedings, NPL, 8-9 April 1974, IPC, London, 1974, *3*.
19. Chuang, T.-J.; Mai Y.-W. Flexural behavior of strain-softening solids. *Int. J. Solids Struct.* **1989**, *25*, *12*, 1427-43.
20. Foster, G. C. Tensile and Flexure Strength of Unidirectional Fiber-Reinforced Composites: Direct Numerical Simulations and Analytic Models, Thesis submitted to the Faculty of the Virginia Polytechnic Institute and State University in partial fulfillment of the requirements for the degree of Master of Science in Engineering Mechanics, February 20, 1998 Blacksburg, Virginia.
21. Calard, V.; Lamon, J. Failure of fibres bundles. *Composites Science and Technology* **2004**, *64*, 701-710.
22. Calard, V. Approches statistiques-probabilistes du comportement mécanique des composites à matrice céramique, Ph.D. Thesis, University of Bordeaux, n° 1948, 199
23. Calard, V.; Lamon J. A probabilistic approach to the ultimate failure of ceramic-matrix composites-part I:Nexperimental investigation of 2D woven SiC/SiC composite. *Composites Science and Technology* **2002**, *62*, *3*, pp. 385-393.
24. Lamon, J.; R'Mili, M. Investigation of flaw strength distributions from tensile force-strain curves of fiber tows. *Composites: Part A* **2021**,145, 106262. doi.org/10.1016/j.compositesa.2020.106262
25. Weibull, W. A statistical distribution function of wide applicability. *J Appl Mech* **1951**, *18*, 293–7.
26. R'Mili, M.; Godin, N.; Lamon, J. Flaw strength distributions and statistical parameters for ceramic fibers: The normal distribution. *Physical Review E* **2012**, *85*, *5*, pp. 1106-1112.
27. Inghels, E.; Lamon, J. An approach to the mechanical behavior of SiC/SiC and C/SiC ceramic matrix composites. 1- Experimental results. *J. Material Science* **1991**, *26*, pp. 5403-5410.
28. Lamon, J. Brittle fracture and damage of brittle materials and compsites: statistical – probabilistic approaches. London, Elsevier Ltd, Oxford, UK: ISTE Press Ltd; 2016.
29. Wisnom, M. R. The effect on specimen size on the bending strength of unidirectional carbon fiber-epoxy. *Compos. Struct*., **1991**, *18*, *1*, pp. 47-63.

 doi:10.20944/preprints202504.2272.v1

30. Wisnom, M. R. Relationship between strength variability and size effect in unidirectionall carbon fiber/epoxy, Composites **1991**, *22*, pp. 47-52.
31. Lamon, J. The Unstable Fracture of Multifilament Tows. J. *Compos. Sci.* **2024**, 8, 52. https://doi.org/10.3390/cs8020052
32. Lamon, J.; R'Mili, M. Investigation of Specimen Size Effectson P-Quantile Diagrams and Normal Distributions of CriticalFlaw Strengths in Fiber Tows. *J. Compos. Sci.* **2022**, 6, 171. https://doi.org/10.3390/jcs6060171